





## PAPER



Cite this: *J. Mater. Chem. B*, 2023, 11, 8271

## Synthesis, nanostructuring and *in silico* studies of a new imine bond containing a macroheterocycle as a promising PBP-2a non- $\beta$ -lactam inhibitor†

Alakbar Huseynzada, \*<sup>acep</sup> Mirjavid Aghayev, <sup>d</sup> Sarvinaz Hajiyeva, <sup>aq</sup>  
Aygun Israyilova, <sup>b</sup> Koray Sayin, <sup>g</sup> Eldar Gasimov, <sup>n</sup> Fuad Rzayev, <sup>i</sup>  
Ulviyya Hasanova, <sup>acp</sup> Goncha Eyvazova, <sup>j</sup> Vagif Abbasov, <sup>k</sup> Zarema Gakhramanova, <sup>c</sup>  
Sanam Huseynova, <sup>o</sup> Parvana Huseynova, <sup>l</sup> Lala Huseynova<sup>m</sup> and Nigar Salimova<sup>n</sup>

This study is devoted to the synthesis of a 40-membered macroheterocycle with its further nanostructuring by magnetite nanoparticles. The mentioned macroheterocycle was synthesized by the [2+2] cyclocondensation of the oxygen-containing diamine with an aromatic dialdehyde in a non-catalytic medium and with no work-up procedure. The structure of the obtained macroheterocycle was studied by <sup>1</sup>H and <sup>13</sup>C nuclear magnetic resonance spectroscopy and matrix-assisted laser desorption/ionization-time of flight mass spectrometry. Furthermore, the nanosupramolecular complex of macroheterocycles with magnetite nanoparticles was obtained and investigated by Fourier-transform infrared and ultraviolet-visible spectroscopy methods. Shifts in the infrared spectra of the nanosupramolecular complex indicate the interaction through metal-aromatic ring non-covalent bonding. The shift is also observed for the C–O–C stretching band of ether bonds. The loading rate of macroheterocycles on magnetite nanoparticles was 18.6%. The morphology of the ensemble was studied by transmission electron microscopy, which confirmed the synthesis of nanospherical particles with a diameter range of 10–20 nm. Powder X-ray diffraction analysis showed patterns of cubic Fe<sub>3</sub>O<sub>4</sub> nanoparticles with a crystallite size equal to 9.1 nm. The macroheterocycle and its nanosupramolecular complex were tested against *Klebsiella pneumoniae*, *Pseudomonas aeruginosa* and *Staphylococcus aureus*. The results have shown that the created complex has shown 64 times better activity against *Staphylococcus aureus* in comparison with the individual macroheterocycle and 32 times better activity in comparison with the pristine antibiotic Ampicillin as a control. In addition, computational analysis of the macroheterocycle was performed at the B3LYP/6-31G level in water. Molecular docking analyses for the macroheterocycle revealed Penicillin-binding protein PBP2a (5M18) from the transpeptidase family as a target protein in *Staphylococcus aureus*.

Received 21st March 2023,  
Accepted 1st August 2023

DOI: 10.1039/d3tb00602f

rsc.li/materials-b

<sup>a</sup> ICRL, Baku State University, Z. Khalilov 23, Baku, AZ 1148, Azerbaijan

<sup>b</sup> Laboratory of Microbiology and Virology, Baku State University, Z. Khalilov 23, Baku, AZ 1148, Azerbaijan

<sup>c</sup> GPOGC SRI, Azerbaijan State Oil and Industry University, Baku, AZ 1010, Azerbaijan. E-mail: alakbar.huseynzada1117@gmail.com

<sup>d</sup> Department of Pharmaceutical Sciences, Northeast Ohio Medical University, 4209 St, OH-44, Rootstown, OH 44272, USA

<sup>e</sup> Chemistry Department, Azerbaijan Engineers Union, Bashir Safarov 118, Baku, AZ 1009, Azerbaijan

<sup>f</sup> Research Institute of Crop Husbandry, Ministry of Agriculture, Baku, AZ 1098, Azerbaijan

<sup>g</sup> Chemistry Department, Faculty of Science, Sivas Cumhuriyet University, Sivas, 58140, Turkey

<sup>h</sup> Department of Cytology, Embryology and Histology, Azerbaijan Medical University, 163 A Samad Vurgun, Baku AZ1078, Azerbaijan

<sup>i</sup> Laboratory of Electron Microscopy of the SRC, Azerbaijan Medical University, 163 A Samad Vurgun, Baku AZ1078, Azerbaijan

<sup>j</sup> Nanoresearch Center, Baku State University, Z. Khalilov 23, Baku, AZ 1148, Azerbaijan

<sup>k</sup> Institute of Petrochemical Processes, K. Avenue 30, Baku, AZ 1005, Azerbaijan

<sup>l</sup> Chemistry Department, Ganja State University, H. Aliyev 429, Ganja, AZ 2001, Azerbaijan

<sup>m</sup> Industrial Safety and Labor Protection Department, Azerbaijan State Oil and Industry University, Baku, AZ 1010, Azerbaijan

<sup>n</sup> Petrochemical Technology and Industrial Ecology Department, Azerbaijan State Oil and Industry University, Baku, AZ 1010, Azerbaijan

<sup>o</sup> Department of Molecular Biology and Biotechnology, Baku State University, Z. Khalilov 23, Baku, AZ 1148, Azerbaijan

<sup>p</sup> ICESCO Biomedical Materials Department, Baku State University, Z. Khalilov 23, Baku, AZ 1148, Azerbaijan

<sup>q</sup> Physics Department, Kent State University, 800 E. Summit St., Kent, OH 44242, USA

† Electronic supplementary information (ESI) available. See DOI: <https://doi.org/10.1039/d3tb00602f>

## Introduction

The use of large organic cyclic molecules in medicine is often limited due to their hydrophobicity, low bioavailability, high toxicity, or low therapeutic index.<sup>1–3</sup> To solve this issue, various methodologies are used among which the non-covalent complexation of nanoparticles with macrocyclic compounds has received increasing attention. The combination of nanoparticles with synthetic organic compounds, especially macroheterocycles, has great potential for application as a catalyst, drug or drug carrier, sensor, templates for synthesis, *etc.*<sup>4–8</sup> This wide range of applications is explained by the unique self-assembled architecture that is congregated *via* non-covalent interaction between nanoparticles and macrocycles, which is also highly dependent on the presence of functional groups and the size of the macrocyclic cavity.<sup>9</sup> The specific spatial arrangement of formed architecture provides a high affinity to certain ions, guest molecules or receptors. The affinity of supramolecular structures toward specific ions or biological structures can be purposefully changed by the introduction of small molecules, ions, metals/metal oxides, nanoparticles, *etc.*<sup>10</sup> This post-self-assembly modification approach, inspired by nature, occurred post-translational modification, received relevance in the last decade and led to the creation of a series of new functionalized materials. The process commonly takes place through non-covalent interactions such as host–guest complexation, van der Waals forces, hydrogen bonding, hydrophilic/hydrophobic and  $\pi$ – $\pi$  stacking.<sup>11–13</sup> Thus, nanostructuring allows the creation of a system (ensemble) whose functions can be much better than the functions of its individual elements separately. An obvious example of it is the recent study<sup>14</sup> that described the efficient preparation of a new MRI agent based on dendrimers and magnetite nanoparticles and the addition of dendrimers to the formulation facilitates the targeting properties of the ensemble. In other words, nanostructuring can change the properties of each individual element by combining them inside one complex system.<sup>15,16</sup> The biological activity of such kinds of ensembles is difficult to predict and often demonstrates extraordinary patterns. Case in point, the biological activity can be very high on the specific strain of the bacteria or be increased in comparison with separate components of the ensemble.<sup>17–19</sup> An example of such type of improvement is the nanostructuring of macroheterocyclic drugs rifampicin and rifabutin, which made possible the enhancement of macrophage uptake and antimycobacterial activity.<sup>20–22</sup>

Different nanoparticles are used for nanostructuring among which magnetite nanoparticles attract special attention. This is caused by the superiority of magnetite nanoparticles, which, in comparison with others, is justified by their proven biocompatibility, well uniformity in size and shape, and effective use as a drug carrier in drug delivery systems.<sup>23</sup> In addition, magnetite recommended itself as a reliable drug delivery system, for instance, in the case of the antitumor drug 5-Fluorouracil.<sup>24</sup>

From the other point, the synthesis of large number-membered macrocycles is restricted by a low yield, and harsh reaction conditions, *i.e.* precise temperature, high dilution factor, solvent

choice, template effect and use of catalysts. Besides this, cyclization reactions concur with polymerization reactions, which affect the yield of the macrocycle product.<sup>25–27</sup> Therefore, most of the synthesis methods of supramolecular compounds require the use of expensive catalysts and metal-based compounds as templates.<sup>28,29</sup> As a result, the development of cheap methods for macroheterocycle formation is in trend for organic chemists.

The molecular docking method may be used to simulate the atomic-level interaction between a tiny molecule and a protein, allowing us to define how small molecules behave in the binding site of our target proteins and to better understand basic biological processes. That's why after its first usage in 1982, popularity increased gradually and now it is used approximately in all biological experiments.<sup>30,31</sup>

*Staphylococcus aureus* is an opportunistic Gram-positive bacteria that are commonly found in the microbiota of the human body. In some circumstances, this class of bacteria can cause severe infections and even lead to death if not treated properly. Due to fast evolution and misuse of antibiotics, *Staphylococcus aureus* has developed a resistance to the known antibacterial agents. MRSA (Methicillin-resistant *Staphylococcus aureus*) strain is resistant to oxacillin (MIC > 4  $\mu\text{g mL}^{-1}$ ), due to the *mecA/mecC* gene, which is responsible for the production of PBP2a/2c proteins. These proteins decrease the binding affinity to  $\beta$ -lactam antibiotics, resulting in antimicrobial resistance.<sup>32,33</sup> Diverse resistance mechanisms (efflux pumps, low-affinity PBPs,  $\beta$ -lactamases, *etc.*) that *Staphylococcus aureus* strains have evolved through the years make it difficult to create new effective antimicrobials toward them. Furthermore, most of those antibacterial drugs that have been licensed in recent years for clinical use (*i.e.* Ceftobiprole, Ceftriaxone, Telavancin, Dalbavancin, Oritavancin, Tedizolid, Omadacycline, and Delafloxacin) cannot be prescribed or have limitation in the treatment of infants.<sup>34</sup> Resistant *Staphylococcus aureus* strains are extremely dangerous for hospitalized newborn infants, urgent care, cancer and immune-compromised patients.<sup>35–38</sup> Considering all those mentioned above, the synthesis and molecular docking of new antibacterial drugs, such as furosemide analogues, non- $\beta$ -lactam allosteric inhibitors or cephalosporins, targeting PBPs has great significance in fighting with antimicrobial resistance.<sup>39,40</sup>

Considering the above-mentioned, the non-catalytic synthesis of a new 40-membered macroheterocycle (MHC3) was performed with further adsorption of it on the surface of magnetite nanoparticles, which was studied by TEM, XRD, FTIR and UV methods. The loading rate of MHC3 on nanoparticles was calculated. The biological activity of the formed nanosupramolecular ensemble and macroheterocycle alone was tested on bacterial strains of *Klebsiella pneumoniae*, *Pseudomonas aeruginosa* and *Staphylococcus aureus* via the serial microdilution method and the results were compared with the activity of the known drug Ampicillin. In order to explain the activity of the MHC3, molecular docking analysis was performed and the target protein for MHC3 in *S. aureus* is the PBP2a (5M18).

## Results and discussion

### Chemical synthesis and investigation.

The synthesis of 40-membered MHC3 was performed by [2+2] cyclocondensation of dialdehyde **1** with diamine **2** at room temperature in an ethanolic solution in a non-catalytic medium (Scheme 2). Formed during the reaction, the yellowish precipitate doesn't need any work-up procedure for purification, just must be washed with distilled water. The dried precipitate was analyzed by  $^1\text{H}$  and  $^{13}\text{C}$  NMR spectroscopy. The detailed analysis of both spectra didn't reveal the presence of a free amine or aldehyde group signal (Fig. S3 and S4, ESI $^\dagger$ ). Instead of them, the signal of imine proton ( $\text{CH}=\text{N}$ ) was observed at  $^1\text{H}$  and  $^{13}\text{C}$  NMR spectra at 8.58 and 157.08 ppm respectively, according to which it is possible to conclude that a cyclocondensation reaction occurred. Taking under advisement this one, it was assumed that the reaction could proceed in two directions (Fig. 1):

1. Interaction of dialdehyde **1** with diamine **2** in the ratio 1:1 ([1+1] cyclocondensation) with the formation of 20 membered macroheterocycle **4**.
2. Interaction of dialdehyde **1** with diamine **2** in the ratio 2:2 ([2+2] cyclocondensation) with the formation of 40-membered macroheterocycle **3** (MHC3).

The possibility of proceeding of [3+3] (or even more) cyclocondensation reaction was not considered, since these products will have a very complex structure and under normal conditions, their formation will be impossible.

Since the same fragment will be seen in the NMR spectra of both molecules (Fig. 2), it will not be possible to distinguish these two molecules based on them.

Considering the above-mentioned, it was decided to do MALDI investigations, which allow the determination of the precise molecular weight of the investigated sample according

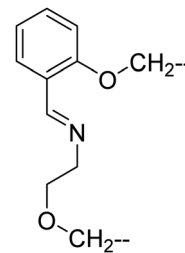


Fig. 2 The fragment that will be seen in the NMR spectra of both **3** and **4** molecules.

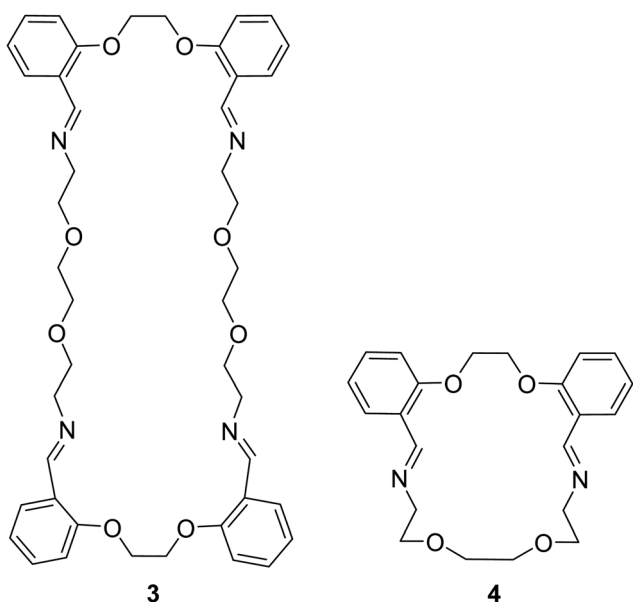


Fig. 1 Two assumed products of the cyclocondensation reaction.

to which it is possible to differentiate the above-mentioned two molecules (Fig. 1). MALDI investigations demonstrated that the molecular weight of the investigated sample is 764 (Fig. S5, ESI $^\dagger$ ). Thus, it is possible to conclude that the [2+2] cyclocondensation reaction occurred with the formation of product **3**, 40-membered macroheterocycle MHC3.

Afterwards, the synthesis of magnetite nanoparticles was performed by a wet chemical co-precipitation method.<sup>42,43</sup> The nanostructuring of MCH3 with obtained magnetite nanoparticles was done by ultrasonic dispersion of nanoparticles in ethanol solution followed by the addition of MCH3 and further stirring of the ultimate solution for a prolonged time. The crystalline structure and purity of synthesized nanosupramolecular complex MHC3@Fe<sub>3</sub>O<sub>4</sub> were characterized by PXRD (Fig. 3). The analyzed sample showed patterns that can be referred to as Fe<sub>3</sub>O<sub>4</sub> nanoparticles of cubic structure. The characteristic peaks of MHC3@Fe<sub>3</sub>O<sub>4</sub> at 12.6 (111), 30.13° (220), 35.536° (311), 43.17° (400), 57.07° (511), 62.75° (440) correlate with the standard pattern of Fe<sub>3</sub>O<sub>4</sub>, indexed in the ICDD (PDF-2/Release 2011 RDB) DB card number 01-075-0449 for the magnetite phase (Table S1, ESI $^\dagger$ ) and with results of recent studies.<sup>53,54</sup> There was no superlattice diffraction observed at 210, 213 and 300, indicating the absence of a maghemite phase. It can be concluded that no phase change occurs due to the functionalization of Fe<sub>3</sub>O<sub>4</sub> by MHC3. Furthermore, no change was observed, which confirms that functionalization with organic moieties did not affect the magnetite phase.<sup>54</sup>

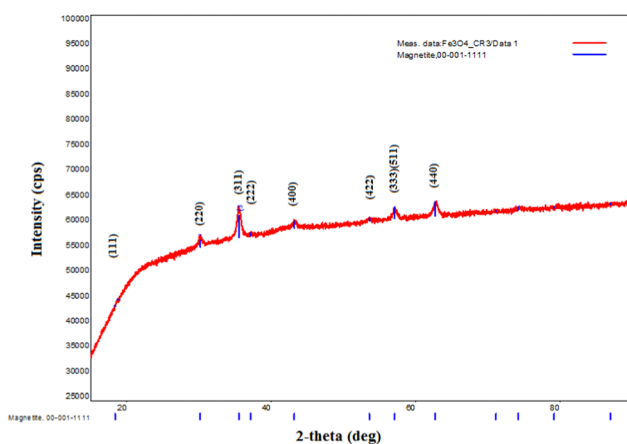


Fig. 3 XRD pattern of the MHC3@Fe<sub>3</sub>O<sub>4</sub> nanosupramolecular complex.

The Williamson–Hall method was used to calculate the crystallite size of the complex based on the most intensive diffraction peak (311). The average crystallite size is 9.1 nm (Table S2, ESI†).

The structure of the MHC3@Fe<sub>3</sub>O<sub>4</sub> nanosupramolecular complex was also studied by FTIR spectroscopy. Fig. S6 (ESI†) demonstrates the spectrum of MHC3.

The peaks corresponding to the aromatic rings are present at 2862 cm<sup>-1</sup> (C–H stretching), 1581 cm<sup>-1</sup> (C=C stretching), 1238 cm<sup>-1</sup> (Ph–O–C stretching), 1087 cm<sup>-1</sup> (in-plane C–H bending), 750 and 929 cm<sup>-1</sup> (out-of-plane C–H bands). The characteristic imine bond peak can be seen at 1636 cm<sup>-1</sup> (CH=N stretching), whereas the ether bond position corresponds to 1162 cm<sup>-1</sup> (C–O–C stretching). Looking at the FTIR spectrum of magnetite nanoparticles (Fig. S7, ESI†), the strong band at 542 cm<sup>-1</sup> corresponds to Fe–O stretching vibrations, whereas peaks at 3400, 2964 and 2899 cm<sup>-1</sup> relate to hydrogen bonding.<sup>55</sup> By comparing the above-described spectra with those of the MHC3@Fe<sub>3</sub>O<sub>4</sub> nanosupramolecular complex (Fig. S8, ESI†), the shifts in several bands can be observed. Absorption values corresponding to the aromatic C=C stretching vibration and Ph–O–C stretching bending have shifted to 1532 cm<sup>-1</sup> and 1096 cm<sup>-1</sup> respectively, indexing on the possible metal–aromatic ring interaction. The shift is also observed for the C–O–C stretching band of ether bonds (1157).

The loading rate of MHC3 on the surface of Fe<sub>3</sub>O<sub>4</sub> was calculated by the Beer–Lambert–Bouguer law. In detail, the standard solutions of MHC3 of known concentrations were prepared and analyzed at 255 nm. The calibration curve was created according to the received results. Then, the concentration of the supernatant, received after the synthesis of MHC3@Fe<sub>3</sub>O<sub>4</sub>, was calculated (Fig. 4). The difference between the amount of MHC3 (mg) before the reaction and the amount of MHC3 in the supernatant is equal to the amount of MHC3, loaded on the surface of Fe<sub>3</sub>O<sub>4</sub> NPs.<sup>56</sup> As a result, it was found that the loading rate of MHC3 on the surface of Fe<sub>3</sub>O<sub>4</sub> was 18.6%.

Furthermore, the morphology of the ensemble MHC3@Fe<sub>3</sub>O<sub>4</sub> was studied by TEM,<sup>57</sup> which demonstrates nanoparticles of the spherical form in the narrow size distribution of 10–20 nm in diameter (Fig. 5). The agglomeration of nanoparticles can occur due to the interaction with the MHC3 supramolecular compound.<sup>43</sup>

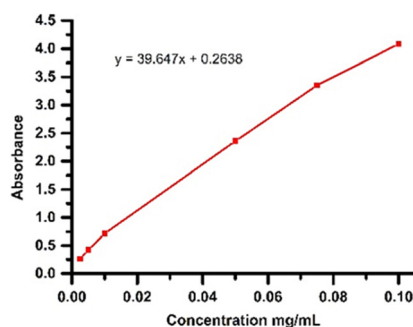


Fig. 4 Standard calibration curve for MHC3.

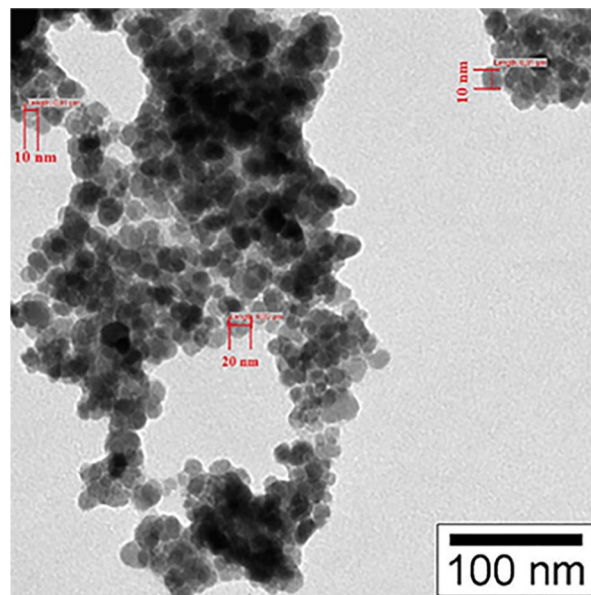


Fig. 5 TEM image of MHC3@Fe<sub>3</sub>O<sub>4</sub> nanosupramolecular complex vibration to 1247 cm<sup>-1</sup>, and in-plane C–H.

**Biological activity.** The next step of the research is the investigation of the biological activity of individual MCH3 and MHC3@Fe<sub>3</sub>O<sub>4</sub> nanosupramolecular complex against *Staphylococcus aureus*, *Pseudomonas aeruginosa* and *Klebsiella pneumoniae*. As shown in Table 1, *S. aureus* was more susceptible against macroheterocycle and nanosupramolecular ensemble in comparison with other bacterial strains. Any inhibition was not detected for pure iron nanoparticles (Fe<sub>3</sub>O<sub>4</sub>) against all bacterial strains, while MHC3@Fe<sub>3</sub>O<sub>4</sub> exhibited low potential activity against Gram-negative bacteria (*K. pneumoniae* and *P. aeruginosa*). The nano supramolecular ensemble (MHC3@Fe<sub>3</sub>O<sub>4</sub>) exhibited the highest inhibition activity (0.5 μg mL<sup>-1</sup>) against *S. aureus*, compared with the MHC3 (32 μg mL<sup>-1</sup>). MHC3 demonstrates high activity at a concentration of 8 μg mL<sup>-1</sup> against *S. aureus*. In this case, we decreased the concentration from 8 to 0.0625 to determine the MIC value for MHC3.

Moreover, the MIC value of MHC3 for *P. aeruginosa* was two times lower than that of ampicillin (516 μg mL<sup>-1</sup>) and was equal to 256 μg mL<sup>-1</sup>. In the case of *K. pneumoniae* MHC3 and the control, the antibiotic showed similar activity with an MIC value of 516 μg mL<sup>-1</sup>. From the results, it was assumed that these Gram-negative bacterial strains are resistant to ampicillin. So, compared with the antibiotic, the macroheterocycle showed better or similar activity against test cultures.

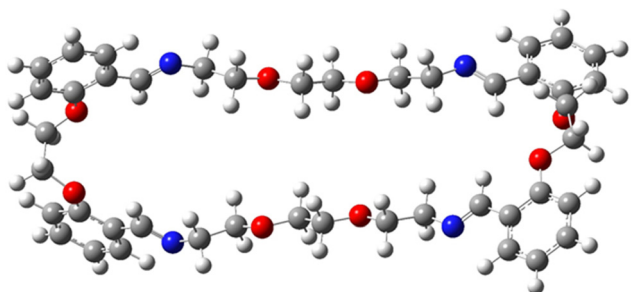
The obtained results revealed that the MIC of the MHC3@Fe<sub>3</sub>O<sub>4</sub> in the case of *S. aureus* (0.5 μg mL<sup>-1</sup>) was lower than the MIC of β-lactam antibiotic (16 μg mL<sup>-1</sup>).

Statistical analyses of the received results of the antimicrobial activity test are given in ESI† (Fig. S9, S10 and Tables S3, S4).

**In silico studies.** MHC3 is optimized at the B3LYP/6-31G level in water. The optimized structure of it is presented in Fig. 6. In the calculation result, no imaginary frequency is

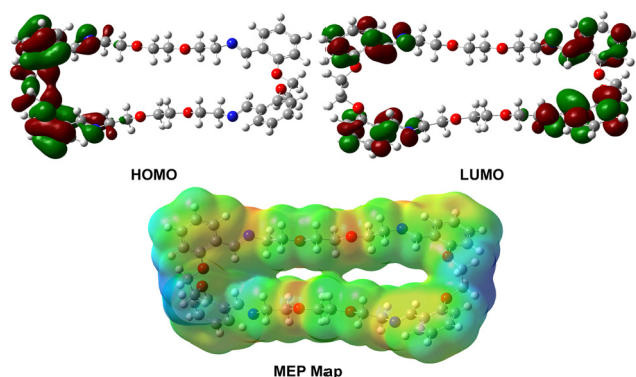
**Table 1** Antibacterial effect of tested compounds on different bacterial strains

Bacterial strains	MIC ( $\mu\text{g mL}^{-1}$ )			
	MHC3	MHC3@Fe <sub>3</sub> O <sub>4</sub> nanoparticles	Fe <sub>3</sub> O <sub>4</sub>	Ampicillin
<i>Klebsiella pneumoniae</i>	512	> 1024	—	512
<i>Pseudomonas aeruginosa</i>	256	1024	—	512
<i>Staphylococcus aureus</i>	32	0.5	—	16

**Fig. 6** Optimized structure of MHC3 at the B3LYP/6-31G level in water.

observed, which means that the calculated structure is stable at the ground state. Electronic properties are investigated and the contour diagram of frontier molecular orbitals and molecular electrostatic potential map of MHC3 are presented in Fig. 7.

According to Fig. 7, there are a lot of red and green balloons in the environment of the benzene ring. Therefore, it can be said that benzene rings can be active for the interaction. As for the MEP map, there are a lot of colours on the surface of the studied compound, among which blue, green and red are the dominant colours. The blue colour means electron-poor regions while the red one means the electron-rich region. Finally, green is in the middle of the blue and red ones. As it can be seen from the MEP map (Fig. 7), the red colour is dominant in the environment of heteroatoms, while the yellow colour is dominant on the benzene surface. In addition to these results, the blue colour is dominant only in the environment of hydrogen atoms.

**Fig. 7** Contour plot of the HOMO, LUMO and MEP map of MHC3.**Table 2** The energy values (eV) of frontier molecular orbitals and energy gap

Compound	$E_{\text{HOMO}}$	$E_{\text{LUMO}}$	$E_{\text{Gap}}$
MHC3	-0.22156	-0.04731	0.17425

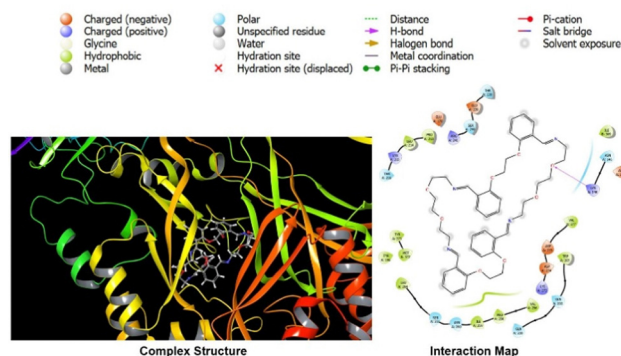
Table 2 presents the calculated energy levels (in eV) of the HOMO and LUMO and the energy gap for the studied compound.

Experimentally, MHC3 has represented the best effect on *Staphylococcus aureus* (Table 1). Thus, molecular docking analyses are performed against *Staphylococcus aureus*. The related protein is downloaded from the protein data bank as 5M18. MHC3 and the related target protein are re-minimized using Maestro 12.8 software.

Then, the  $x$ - $y$ - $z$  coordinate of the receptor binding domain is defined as 19.62, -17.89, and -52.91, respectively. Molecular docking calculations are performed. The complex structure and interaction map are shown in Fig. 8.

According to Fig. 8, MHC3 is docked with the target protein, 5M18. The docking score, van der Waals interaction energy, Coulomb interaction energy and total interaction energy are calculated as -3.492, -42.935, -7.021 and -49.956 kcal mol<sup>-1</sup>, respectively. The key-lock harmony between the inhibitor and protein can be associated with the docking score. The more negative the docking score, the better the harmony between the inhibitor and protein. Thus, due to the fact that the total interaction energy is negative, the interaction between protein and ligand is good, which implies that there is a stable interaction between the studied compound and the target protein. Amino acid sequences interacting with the inhibitor are given in the part of the inhibitor up to a distance of 4 Å in the interaction map. There are different colours on the amino acids in the interaction map and the mean of these colours is given above in Fig. 8. Red and purple colours are related to the physical interaction while the other ones are related to the weak chemical interactions.

Amino acid residues include: ASN 146, LYS 148, GLU 170, TYR 196, GLN 200, GLN 203, TRP 205, PRO 213, LEU 214, LYS 215, THR 216, THR 238, GLU 239, SER 240, ARG 241, VAL 256, PRO 258, ILE 259, ASN 260, SER 261, LEU 264, LYS 273, ASP

**Fig. 8** The complex structure and interaction map between MHC3 and 5M18.

274, ASP 275, VAL 277, ASP 295, ILE 309, MET 372, and TYR 373. Based on the fact that the allosteric binding pocket contains residues 166–240, 258–277 and 364–390, it can be concluded that the MHC3 binds non-covalently to the allosteric site. The allosteric site inhibitors act by non-covalently binding and changing the conformation of the allosteric site, which in turn leads to the opening of the active site.<sup>39,65</sup>

The non-covalent binding takes place through a hydrogen bond between Lys148 and a lone pair of oxygen in MHC3. The hydrophobic interactions are present between the phenyl ring, ether bridges of MHC3 and Val256, Pro258, and Ile259 of 5M18. Polar interactions in the regions of Asn146 and Lys148 with MHC3 are also shown, which can also be explained by the presence of unshared electron pairs of heteroatoms (oxygen and nitrogen in the imine bond) in the structure of the inhibitor and amino groups in these amino acids.

It is known that *S. aureus* is a Gram-positive bacteria that cause skin and respiratory infections. It is considered one of the major threats to human health, because of its intrinsic or acquired resistance to the available antibiotics and treatments. Penicillins were the first line of antibiotics that were used in the treatment of infections rendered by *S. aureus*.<sup>58,59</sup> These antibiotics kill bacteria by inhibiting the enzymes that are involved in the pathway of cell wall synthesis in Gram-positive bacteria. Penicillins kill bacteria by inhibiting the enzymes that are involved in the pathway of the synthesis of peptidoglycan, the principal building block of the bacterial cell wall.<sup>60–62</sup> Transpeptidases – penicillin-binding proteins (PBPs) carried out the synthesis of peptidoglycan by the crosslinking reaction. PBP activity is crucial for bacterial survival, making them an attractive target for designing new antibacterial drugs.<sup>63,64</sup> There are four native penicillin-binding proteins found in *S. aureus*: PBP1, PBP2, PBP3 and PBP4.<sup>58</sup> PBP2a (5M18) is a special protein that is not effectively inhibited by  $\beta$ -lactams and it is an Achilles' heel of methicillin-resistant *Staphylococcus aureus*.<sup>65</sup> For this reason, PBP2a is an attractive drug target in order to design new generation antibacterials that will help to combat resistant bacterial strains.<sup>58–64</sup>

The obtained results from the *in silico* analysis revealed that the target protein for MHC3 in *S. aureus* is the PBP2a (5M18). In future, this molecule can be applied as a non- $\beta$ -lactam antibiotic, which will provide keys for the development of future compounds that block the interaction of PBP2a with its target.<sup>65</sup>

## Experimental

### Materials and methods

All the solvents and reagents were purchased from commercial suppliers and were of analytical grade and used without further purification. The control of the reactions' progress and the determination of the synthesized compound purity were done by thin-layer chromatography (TLC) on Merck silica gel plates (60 F254 aluminium sheets) which were visualized under UV light. Melting points were recorded in open capillary tubes on

Buchi B-540 apparatus and were uncorrected. Elemental analysis was performed on a Carlo Erba 1108 analyzer.

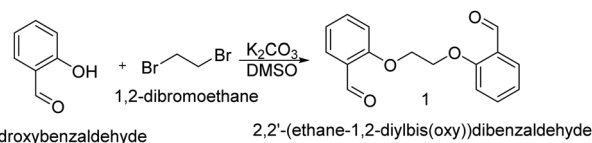
### Synthetic procedures

#### Synthesis of 2,2'-(ethane-1,2-diylbis(oxy))dibenzaldehyde.

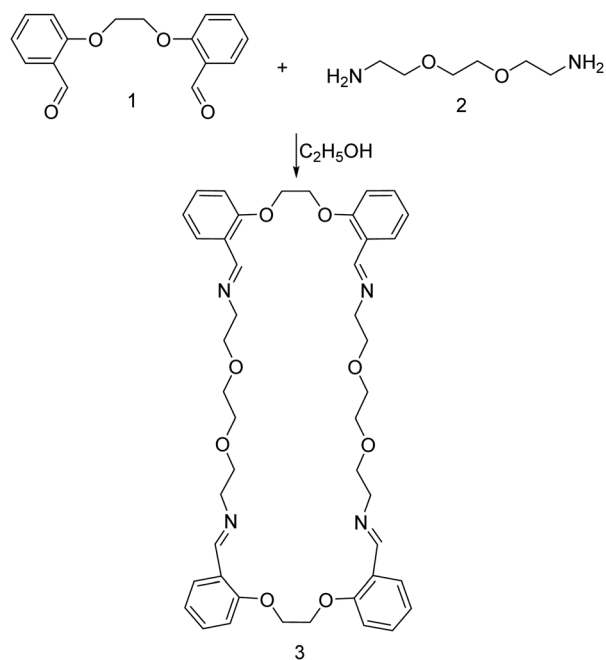
The synthesis of dialdehyde **1** was done according to the known literature method.<sup>41</sup> In detail, 37.7 mmol of  $K_2CO_3$  was added to a solution of 38.3 mmol of salicylaldehyde in 20 mL DMSO. Subsequently, after adding 19.8 mmol of 1,2-dibromoethane, the reaction mixture was heated in a water bath for 3.5 h (Scheme 1). At the end of the mentioned time, the reaction mixture was poured on ice and left for 3 h. The formed precipitate was filtered, washed with distilled water, and dried. Afterwards, it was washed with  $CCl_4$  till the bleaching of the precipitate colour and dried at room temperature. The yield is 70%, m.p. 116–118 °C.  $^1H$  NMR spectrum (Fig. S1, ESI<sup>†</sup>) of compound **1**: (DMSO- $d_6$ ,  $\delta$ , ppm), 4.57 s (4H, 2OCH<sub>2</sub>), 7.07–7.12 t (2H, Ar,  $J$  = 9 Hz), 7.31–7.34 d (2H, Ar,  $J$  = 9 Hz), 7.64–7.69 t (4H, Ar,  $J$  = 9 Hz), 10.29 s (2H, COH).  $^{13}C$  NMR spectrum (Fig. S2, ESI<sup>†</sup>) of compound **1**: (DMSO- $d_6$ ,  $\delta$ , ppm), 67.87 (2OCH<sub>2</sub>), 114.61 (2CH, Ar), 121.58 (2CH, Ar), 124.97 (2C, Ar), 128.02 (2CH, Ar), 136.85 (2CH, Ar), 161.28 (2C, Ar), 189.60 (2COH). Found, %: C 71.04; H 5.11.  $C_{16}H_{14}O_4$ . Calculated, %: C 71.11; H 5.19.

**Synthesis of 6,7,15,16,18,19,21,22,30,31,39,40,42,43,45,46-hexadecahydrotetraazabenzoc[*c*,*i*,*i*,*o*][1,4,11,14,21,24,31,34]octa-oxa[7,18,27,38]tetraazacyclotetracontine (MHC3).** 0.37 mmol of dialdehyde **1** was dissolved in 5 mL of hot ethanol. Subsequently, 1.37 mmol of 2,2'-(ethylenedioxy)bis(ethylamine) was added to the reaction mixture and vigorously stirred for an hour (Scheme 2). At the end of reaction time, the ethanolic solution was poured into an ice–water mixture and left for 10 minutes. Afterwards, the solution was vigorously stirred with the addition of sodium chloride and the yellowish precipitate is formed, which was filtered, washed with distilled water and dried. Yield 45%, m.p. 148–150 °C.  $^1H$  NMR spectrum (Fig. S3, ESI<sup>†</sup>) of MHC3: (DMSO- $d_6$ ,  $\delta$ , ppm), 3.41 s (10H, 5OCH<sub>2</sub>), 3.62 s (14H, 4NCH<sub>2</sub> + 3OCH<sub>2</sub>), 4.43 s (8H, 4OCH<sub>2</sub>), 6.99–7.03 t (4H, Ar,  $J$  = 6 Hz), 7.14–7.17 d (4H, Ar,  $J$  = 9 Hz), 7.43–7.48 t (4H, Ar,  $J$  = 9 Hz), 7.85–7.88 d (4H, Ar,  $J$  = 9 Hz), 8.58 s (4H, 4CH=N).  $^{13}C$  NMR spectrum (Fig. S4, ESI<sup>†</sup>) of MHC3: (DMSO- $d_6$ ,  $\delta$ , ppm), 61.37 (4NCH<sub>2</sub>), 67.11 (4OCH<sub>2</sub>), 70.11 (4OCH<sub>2</sub>), 70.18 (4OCH<sub>2</sub>), 113.09 (4CH, Ar), 121.19 (4CH, Ar), 124.53 (4C, Ar), 127.11 (4CH, Ar), 132.53 (4CH, Ar), 157.08 (4CH=N), 157.98 (4C, Ar). MALDI-TOF MS = 764.950 (Fig. S5, ESI<sup>†</sup>). Found, %: C 69.01; H 6.91; N 7.39.  $C_{44}H_{52}N_4O_8$ . Calculated, %: C 69.09; H 6.85; N 7.32.

**Synthesis of magnetite nanoparticles and their nanostructuring with MHC3.** Magnetite nanoparticles were synthesized



Scheme 1 Synthesis of dialdehyde **1**.



Scheme 2 Synthesis of macrocycle 3.

by the wet chemical co-precipitation method.<sup>42,43</sup>  $\text{FeSO}_4 \cdot 7\text{H}_2\text{O}$  and  $\text{FeCl}_3 \cdot 10\text{H}_2\text{O}$  were dissolved in distilled water at a weight ratio of 2 : 3 under bubbling of nitrogen gas at 60 °C for 6 hours. After that, the received precipitate was separated by a NdFeB magnet and washed several times with deionized water. In order to synthesize the  $\text{MHC3}@Fe_3O_4$  nanosupramolecular complex, MHC3 and  $Fe_3O_4$  were taken in the ratio of 1 : 2. First, nanoparticles were dispersed in ethanol by ultrasonic irradiation for 15 minutes. Dispersion of the synthesized samples was carried out on a Sonics Vibra Cell sonicator with the following parameters: pulse –30 s (on), 2 s (off); power –40%. Then dissolved in ethanol MHC3 was added to the final solution and the mixture was stirred for 5 hours under a nitrogen atmosphere. Furthermore, the  $\text{MHC3}@Fe_3O_4$  nanosupramolecular complex was separated from ethanol by a NdFeB magnet and dried at ambient temperature. The supernatant was analyzed to determine the loading amount of MHC3.

**Nuclear magnetic resonance (NMR) experiments.** The NMR experiments were performed on a BRUKER FT NMR spectrometer AVANCE 300 (Bruker, Karlsruhe, Germany) (300 MHz for  $^1\text{H}$  and 75 MHz for  $^{13}\text{C}$ ) with a BVT 3200 variable temperature unit in 5 mm sample tubes using Bruker Standard software (TopSpin 3.1). Chemical shifts were given in ppm ( $\delta$ ) and were referenced to internal tetramethylsilane (TMS). Multiplicities are declared as follows: s (singlet), d (doublet), t (triplet), q (quadruplet), and m (multiplet). Coupling constants  $J$  are given in Hz. The experimental parameters for  $^1\text{H}$  are as follows: digital resolution = 0.23 Hz, SWH = 7530 Hz, TD = 32 K, SI = 16 K, 90° pulse-length = 10 ms, PL1 = 3 dB,  $ns = 4$ ,  $ds = 2$ ,  $d1 = 1$  s and for  $^{13}\text{C}$  as follows: digital resolution = 0.27 Hz, SWH = 17985 Hz, TD = 64 K, SI = 32 K, 90° pulse-length = 9 ms, PL1 = 1.5 dB,  $ns = 1000$ ,  $ds = 2$ ,  $d1 = 3$  s. The NMR-grade DMSO- $d_6$

(99.7%, containing 0.3%  $\text{H}_2\text{O}$ ) was used for the solutions of synthesized compounds.

**Mass experiments.** Matrix-assisted laser desorption/ionization-time of flight mass spectrometry (MALDI-TOF MS) analysis was performed using Bruker Microflex LT MALDI-TOF MS equipped with a nitrogen UV-Laser operating at 337 nm. The spectrum was recorded in reflectron modes with an average of 100 shots.  $\alpha$ -cyano-4-hydroxycinnamic acid (CHCA) was used as a MALDI matrix at a concentration of 10  $\text{mg mL}^{-1}$  (methanolic solution). MALDI samples were prepared by mixing sample solution (4  $\text{mg mL}^{-1}$  in methanol) with the matrix solution (1 : 10 v/v) in a 0.5 mL Eppendorf microtube. Finally, 1.0  $\mu\text{L}$  of this mixture was deposited on the sample plate, dried at room temperature, and then analyzed.

**Ultraviolet-visible (UV-vis) experiments.** The loading of MHC3 on the surface of  $Fe_3O_4$  nanoparticles was calculated through the Beer–Lambert–Bouguer law, according to the UV spectra of the compounds. The experiments were done on a UV-Vis Spectrophotometer Specord 250 Plus at 255 nm for standard solutions of MHC3 with different concentrations in the range of 0.1–0.001  $\text{mg mL}^{-1}$ .

**Fourier-transform infrared (FTIR) investigations.** In order to investigate the interactions between MHC3 and  $Fe_3O_4$  in a nanosupramolecular ensemble ( $Fe_3O_4@MHC3$ ) and to determine through which functional groups the non-covalent bonding takes place, the FTIR spectra of MHC3,  $Fe_3O_4$  and  $Fe_3O_4@MHC3$  were recorded on a FTIR spectrometer Thermo Scientific™ Nicolet™ iS20, using an attenuated total reflectance (ATR) accessory in the range of 4000–450  $\text{cm}^{-1}$ .

**X-Ray powder diffraction analysis (PXRD).** XRD analysis was performed under ambient conditions on a Rigaku Mini Flex 600 XRD diffractometer, equipped with  $\text{CuK}\alpha$  radiation, to study the crystalline structure of the synthesized  $Fe_3O_4@MHC3$ . The samples were scanned in the Bragg angle range of 10°–80° at  $2\theta$ , 15 mA. The Williamson–Hall method was used to calculate the crystallite size.

**Transmission electron microscopy (TEM) study.** The TEM analysis of the nanosupramolecular ensemble  $\text{MHC3}@Fe_3O_4$  was performed on a TEM JEOL-1400 (Japan) at 80–120 kV. The ultrasonicated solution of  $\text{MHC3}@Fe_3O_4$  in ethanol was placed on a carbon-coated grid and remained to dry under ambient conditions. Morphometric analysis of the images (electronograms) was carried out, using the TEM Imaging Platform program (Olympus Soft Imaging Solutions GmbH (Germany)).

**Biological assays.** The synthesized macroheterocycle and its supramolecular ensemble on the basis of magnetite nanoparticles were tested by the 96-well microtiter assay on the *Klebsiella pneumoniae*, *Pseudomonas aeruginosa*, and *Staphylococcus aureus*. The bacterial strains used in the microbiological studies were taken from the culture collection of the Department of Microbiology (Baku State University, Azerbaijan). Muller Hinton medium (“Liofilchem”) was used for the inoculation of the fresh colony. Assessed substances were placed into each well of U-bottom microtiter at different concentrations from 1024 to 8  $\mu\text{g mL}^{-1}$  and afterwards, bacterial strains were inoculated into each well in an amount of  $1 \times 10^5$  CFU.

The MHC3 was dissolved in dimethyl sulfoxide and Fe<sub>3</sub>O<sub>4</sub>@MHC3 was dispersed in distilled water by applying sonication for 15 minutes (pulse –30 s (on), 2 s (off); power –40%). The resazurin dye (Sigma Aldrich) was used for the determination of the bacterial growth after incubation for 24 h at 37 °C. 30 µL of resazurin solution (0.01%) was added to each well and the microtiter plates were incubated at 37 °C for additional 4 hours. The colour change from blue to pink is considered as evidence of bacterial growth. This way the minimum inhibitory concentration (MIC) is considered as the concentration after which the tested compounds do not inhibit this change in colour.<sup>44–47</sup>

**Computational studies.** Quantum chemical calculations of MHC3 were performed using Gaussian software.<sup>46–49</sup> B3LYP, one of the DFT hybrid functions, was selected as the calculation method with a 6-31G basis set. All calculations were performed in the water phase and the C-PCM solvent method was used for this purpose. Additionally, molecular docking calculations were performed using the OPLS4 method and Maestro 12.8 software.<sup>50–52</sup>

## Conclusions

The synthesis route without using a catalyst and special reaction conditions was successful for the formation of a pure 40-membered macroheterocycle MCH3 on the basis of the mentioned diamine and dialdehyde. Nanostructuring of macroheterocycles with magnetite nanoparticles was performed and the loading rate of MCH3 on magnetite nanoparticles was 18.6%. The biological activity investigations against *S. aureus*, *P. aeruginosa* and *K. pneumoniae* were performed and in the case of *S. aureus*, MHC3 showed potential activity with an MIC value of 32 µg mL<sup>-1</sup>. The MHC3@Fe<sub>3</sub>O<sub>4</sub> nanostructure showed an MIC value of 0.5 µg mL<sup>-1</sup> on *S. aureus*. The results of computational studies demonstrated that the potent activity sites of MHC3 are predominantly benzene rings with heteroatoms being also susceptible to the interaction. PBP2a (5M18) protein was identified as a target for the synthesized macroheterocycle, thus, the MHC3 can be considered as a promising drug candidate that can act as a non-β-lactam inhibitor of penicillin-binding protein. Future non-lactam antibiotics based on this molecule's potential use will offer insights into how to create drugs that prevent PBP2a from interacting with its target.

## Author contributions

Alakbar Huseynzada: synthesis, NMR and mass investigations, formal analysis, and writing – original draft. Mirjavid Aghayev: synthesis, formal analysis, and writing – review & editing. Sarvinaz Hajiyeva: nanostructuring, powder XRD analysis, formal analysis, writing – original draft, and writing – review & editing. Aygun Israyilova: antibacterial studies, writing – original draft, and writing – review & editing. Koray Sayin: computational approach and writing – original draft. Eldar Gasimov: electron microscopy, writing – original draft, and writing – review & editing. Fuad Rzayev: electron microscopy, writing – original

draft, and writing – review & editing. Ulviyya Hasanova: writing – original draft, supervision, funding acquisition, and project administration. Goncha Eyvazova: UV-spectroscopy, formal analysis, and writing – review & editing. Vagif Abbasov: project administration. Zarema Gakhramanova: and writing – review & editing. Sanam Huseynova: antibacterial studies. Parvana Huseynova: analytical calculations. Lala Huseynova: formal analysis, and writing – review & editing. Nigar Salimova: formal analysis, and writing – review & editing.

## Conflicts of interest

There are no conflicts to declare.

## Acknowledgements

The research was co-funded by the Science Development Foundation under the President of the Azerbaijan Republic and TUBITAK in the frames of project number EİF-BGM-5-AZTURK-1/2018-2/02/4-M-02 and ICESCO.

## Notes and references

- 1 R. C. F. Leonard, S. Williams, A. Tulpule, A. M. Levine and S. Oliveros, *Breast*, 2009, **18**, 218–224, DOI: [10.1016/j.breast.2009.05.004](https://doi.org/10.1016/j.breast.2009.05.004).
- 2 F. Ditzinger, D. J. Price, A. R. Ilie, N. J. Köhl, S. Jankovic, G. Tsakiridou, S. Aleandri, L. Kalantzi, R. Holm, A. Nair, C. Saal, B. Griffin and M. Kuentz, *J. Pharm. Pharmacol.*, 2019, **71**, 464–482, DOI: [10.1111/jphp.12984](https://doi.org/10.1111/jphp.12984).
- 3 X. Zhang, H. Xing, Y. Zhao and Z. Ma, *Pharmaceutics*, 2018, **10**, 74, DOI: [10.3390/pharmaceutics10030074](https://doi.org/10.3390/pharmaceutics10030074).
- 4 J. Jökel, F. Schwer, M. von Delius and U. P. Apfel, *Chem. Commun.*, 2020, **56**, 14179–14182, DOI: [10.1039/D0CC05229A](https://doi.org/10.1039/D0CC05229A).
- 5 N. Pairault, H. Zhu, D. Jansen, A. Huber, C. G. Daniliuc, S. Grimme and J. Niemeyer, *Angew. Chem., Int. Ed.*, 2020, **59**, 5102–5107, DOI: [10.1002/anie.201913781](https://doi.org/10.1002/anie.201913781).
- 6 H. Kumari, A. Eisenhart, J. Pajoubpong, F. Heinrich and T. L. Beck, *RSC Adv.*, 2020, **10**, 15148–15153, DOI: [10.1039/D0RA02850A](https://doi.org/10.1039/D0RA02850A).
- 7 H. Zhu, L. Shangguan, B. Shi, G. Yu and F. Huang, *Mater. Chem. Front.*, 2018, **2**, 2152–2174, DOI: [10.1039/C8QM00314A](https://doi.org/10.1039/C8QM00314A).
- 8 S. Saqib, S. Faryad, M. I. Afridi, B. Arshad, M. Younas, M. Naeem, W. Zaman, F. Ullah, M. Nisar, S. Ali, A. M. Elgorban, A. Syed, H. O. Elansary and T. K. Z. El-Abedin, *Coatings*, 2022, **12**, 1505, DOI: [10.3390/coatings12101505](https://doi.org/10.3390/coatings12101505).
- 9 Y. Geng, M. Liu, J. Xue, P. Xu, Y. Wang, L. Shu, Q. Zeng and C. Wang, *Chem. Commun.*, 2015, **51**, 6820–6823, DOI: [10.1039/C5CC01032B](https://doi.org/10.1039/C5CC01032B).
- 10 M. J. Schotman, P. P. Fransen, J. Song and P. Y. Dankers, *RSC Adv.*, 2022, **12**, 14052–14060, DOI: [10.1039/D2RA00346E](https://doi.org/10.1039/D2RA00346E).
- 11 L. J. Chen and H. B. Yang, *Acc. Chem. Res.*, 2018, **51**, 2699–2710, DOI: [10.1021/acs.accounts.8b00317](https://doi.org/10.1021/acs.accounts.8b00317).



- 12 Y. Yang, J. S. Chen, J. Y. Liu, G. J. Zhao, L. Liu, K. L. Han, T. R. Cook and P. J. Stang, *J. Phys. Chem. Lett.*, 2015, **6**, 1942–1947, DOI: [10.1021/acs.jpcclett.5b00783](https://doi.org/10.1021/acs.jpcclett.5b00783).
- 13 Y. R. Zheng, W. J. Lan, M. Wang, T. R. Cook and P. J. Stang, *J. Am. Chem. Soc.*, 2011, **133**, 17045–17055, DOI: [10.1021/ja207217t](https://doi.org/10.1021/ja207217t).
- 14 J. Yang, Y. Luo, Y. Xu, J. Li, Z. Zhang, H. Wang, M. Shen, X. Shi and G. Zhang, *ACS Appl. Mater. Interfaces*, 2015, **7**, 5420–5428, DOI: [10.1021/am508983n](https://doi.org/10.1021/am508983n).
- 15 R. Yan, Y. Hu, F. Liu, S. Wei, D. Fang, A. J. Shuhendler, H. Liu, H.-Y. Chen and D. Ye, *J. Am. Chem. Soc.*, 2019, **141**, 10331–10341, DOI: [10.1021/jacs.9b03649](https://doi.org/10.1021/jacs.9b03649).
- 16 S. Li, Q. Zou, Y. Li, C. Yuan, R. Xing and X. Yan, *J. Am. Chem. Soc.*, 2018, **140**, 10794–10802, DOI: [10.1021/jacs.8b04912](https://doi.org/10.1021/jacs.8b04912).
- 17 U. A. Hasanova, M. A. Ramazanov, A. M. Maharramov, Z. Gakhramanova, S. F. Hajiyeva, L. Vezirova, G. M. Eyvazova, F. V. Hajiyeva, P. Huseynova and Z. Agamaliyev, *J. Inclusion Phenom. Macrocyclic Chem.*, 2016, **86**, 19–25, DOI: [10.1007/s10847-016-0636-x](https://doi.org/10.1007/s10847-016-0636-x).
- 18 U. Hasanova, M. Ramazanov, A. Maharramov, Z. Gakhramanova, S. Hajiyeva, Q. Eyvazova, L. Vezirova, F. Hajiyeva, M. Hasanova and N. Guliyeva, *Chem. Eng. Trans.*, 2016, **47**, 109–114, DOI: [10.3303/CET1647019](https://doi.org/10.3303/CET1647019).
- 19 S. Hajiyeva, U. Hasanova, Z. Gakhramanova, A. Israyilova, K. Ganbarov, E. Gasimov, F. Rzayev, G. Eyvazova, A. Huseynzada, G. Aliyeva, I. Hasanova & A. Maharramov, *Turk. J. Chem.*, 2019, **43**, 1711–1721, DOI: [10.3906/kim-1907-10](https://doi.org/10.3906/kim-1907-10).
- 20 S. P. Carneiro, K. V. Carvalho, R. D. D. O. A. Soares, C. M. Carneiro, M. H. G. de Andrade, R. S. Duarte and O. D. H. Dos Santos, *Colloids Surf., B*, 2019, **175**, 306–313, DOI: [10.1016/j.colsurfb.2018.12.003](https://doi.org/10.1016/j.colsurfb.2018.12.003).
- 21 H. Rouco, P. Diaz-Rodriguez, D. P. Gaspar, L. M. Gonçalves, M. Cuerva, C. Remuñán-López, A. J. Almeida and M. Landin, *Nanomaterials*, 2020, **10**, 2138, DOI: [10.3390/nano10112138](https://doi.org/10.3390/nano10112138).
- 22 M. Pinheiro, R. Ribeiro, A. Vieira, F. Andrade and S. Reis, *Drug Des., Dev. Ther.*, 2016, **10**, 2467, DOI: [10.2147/DDDT.S104395](https://doi.org/10.2147/DDDT.S104395).
- 23 R. C. F. Leonard, S. Williams, A. Tulpule, A. M. Levine and S. Oliveros, *Breast*, 2009, **18**, 218–224, DOI: [10.1016/j.breast.2009.05.004](https://doi.org/10.1016/j.breast.2009.05.004).
- 24 L. Alupeii, C. A. Peptu, A. M. Lungan, J. Desbrieres, O. Chiscan, S. Radji and M. Popa, *Int. J. Biol. Macromol.*, 2016, **92**, 561–572, DOI: [10.1016/j.ijbiomac.2016.07.058](https://doi.org/10.1016/j.ijbiomac.2016.07.058).
- 25 C. Fan, B. Sun, Z. Li, J. Shi, T. Lin, J. Fan and Z. Shi, *Angew. Chem., Int. Ed.*, 2021, **60**, 13896–13899, DOI: [10.1002/anie.202104090](https://doi.org/10.1002/anie.202104090).
- 26 S. A. Babu, *Tetrahedron*, 2015, **71**, 7758–7781, DOI: [10.1016/j.tet.2015.06.070](https://doi.org/10.1016/j.tet.2015.06.070).
- 27 J. Kang, J. Zhu, J. Lin, C. Han, K. Liu and X. Wang, *Macromolecules*, 2021, **54**, 7441–7447, DOI: [10.1021/acs.macromol.1c01063](https://doi.org/10.1021/acs.macromol.1c01063).
- 28 V. G. Jiménez, A. H. David, J. M. Cuerva, V. Blanco and A. G. Campaña, *Angew. Chem., Int. Ed.*, 2020, **59**, 15124–15128, DOI: [10.1002/anie.202003785](https://doi.org/10.1002/anie.202003785).
- 29 K. V. Lawson, T. E. Rose and P. G. Harran, *Proc. Natl. Acad. Sci. U. S. A.*, 2013, **110**, E3753–E3760, DOI: [10.1073/pnas.1311706110](https://doi.org/10.1073/pnas.1311706110).
- 30 B. J. McConkey, V. Sobolev and M. Edelman, *Curr. Sci.*, 2002, 845–856.
- 31 I. D. Kuntz, J. M. Blaney, S. J. Oatley, R. Langridge and T. E. Ferrin, *J. Mol. Biol.*, 1982, **161**, 269–288, DOI: [10.1016/0022-2836\(82\)90153-X](https://doi.org/10.1016/0022-2836(82)90153-X).
- 32 Y. Uehara, *Antibiotics*, 2022, **11**, 86, DOI: [10.3390/antibiotics11010086](https://doi.org/10.3390/antibiotics11010086).
- 33 Z. Hou, L. Liu, J. Wei and B. Xu, *Infect. Drug Resist.*, 2023, 3271–3292, DOI: [10.2147/IDR.S412308](https://doi.org/10.2147/IDR.S412308).
- 34 S. Esposito, F. Blasi, N. Curtis, S. Kaplan, T. Lazzarotto, M. Meschiari, C. Mussini, M. Peghin, C. Rodrigo, A. Vena, N. Principi and M. Bassetti, *Antibiotics*, 2023, **12**, 742, DOI: [10.3390/antibiotics12040742](https://doi.org/10.3390/antibiotics12040742).
- 35 T. Nakashima, H. Inoue, Y. Sakemi and H. Yamashita, *Infect. Control Hosp. Epidemiol.*, 2023, **44**, 988–990, DOI: [10.1017/ice.2022.150](https://doi.org/10.1017/ice.2022.150).
- 36 N. K. Harrell, K. Tyler, L. Jacob, L. B. Carter, D. Hunt, B. Dart and R. Maxwell, *J. Surg. Res.*, 2023, **285**, 45–50, DOI: [10.1016/j.jss.2022.12.014](https://doi.org/10.1016/j.jss.2022.12.014).
- 37 C. H. Chew, C. C. Yeo, A. M. Che Hamzah, E. A. I. Al-Trad, S. U. Jones, K. H. Chua and S. M. Pua, *Diagnostics*, 2023, **13**, 1050, DOI: [10.3390/diagnostics13061050](https://doi.org/10.3390/diagnostics13061050).
- 38 J. Li, H. Zheng and S. S. Y. Leung, *Sci. Rep.*, 2023, **13**, 9534, DOI: [10.1038/s41598-023-36749-2](https://doi.org/10.1038/s41598-023-36749-2).
- 39 M. F. Harras, R. Sabour, T. A. Farghaly and M. H. Ibrahim, *Bioorg. Chem.*, 2023, **137**, 106585, DOI: [10.1016/j.bioorg.2023.106585](https://doi.org/10.1016/j.bioorg.2023.106585).
- 40 M. A. A. Ibrahim, K. A. A. Abdeljawaad, A. H. M. Abdelrahman, O. R. Alzahrani, F. M. Alshabirmi, E. Khalaf, M. F. Moustafa, F. Alrumaihi, K. S. Allemailem, M. E. S. Soliman, P. W. Paré, M. F. Hegazy and M. A. M. Atia, *Antibiotics*, 2021, **10**, 934, DOI: [10.3390/antibiotics10080934](https://doi.org/10.3390/antibiotics10080934).
- 41 A. M. Maharramov, M. A. Ramazanov, G. A. Guliyeva, A. E. Huseynzada, U. A. Hasanova, N. G. Shikhaliyev, G. M. Eyvazova, S. F. Hajiyeva, I. G. Mamedov and M. M. Aghayev, *J. Mol. Struct.*, 2017, **1141**, 39–43, DOI: [10.1016/j.molstruc.2017.03.084](https://doi.org/10.1016/j.molstruc.2017.03.084).
- 42 R. Massart, *IEEE Trans. Magn.*, 1981, **17**, 1247–1248, DOI: [10.1109/TMAG.1981.1061188](https://doi.org/10.1109/TMAG.1981.1061188).
- 43 S. Saqib, W. Zaman, A. Ayaz, S. Habib, S. Bahadur, S. Hussain, S. Muhammad and F. Ullah, *Biocatal. Agric. Biotechnol.*, 2020, **28**, 101729, DOI: [10.1016/j.bcab.2020.101729](https://doi.org/10.1016/j.bcab.2020.101729).
- 44 A. Martin, H. Takiff, P. Vandamme, J. Swings, J. C. Palomino and F. Portaels, *J. Antimicrob. Chemother.*, 2006, **58**, 327–331, DOI: [10.1093/jac/dkl231](https://doi.org/10.1093/jac/dkl231).
- 45 A. Israyilova, S. Buroni, F. Forneris, V. C. Scoffone, N. Shixaliyev, G. Riccardi and L. R. Chiarelli, *PLoS One*, 2016, **11**, e0167350, DOI: [10.1371/journal.pone.0167350](https://doi.org/10.1371/journal.pone.0167350).
- 46 A. Huseynzada, M. Mori, F. Meneghetti, A. Israyilova, G. Tuzun, K. Sayin, L. R. Chiarelli, C. Mutlu, M. Demiralp, U. Hasanova and V. Abbasov, *J. Mol. Struct.*, 2022, **1267**, 133571, DOI: [10.1016/j.molstruc.2022.133571](https://doi.org/10.1016/j.molstruc.2022.133571).
- 47 A. Huseynzada, C. Jelsch, H. V. Akhundzada, S. Soudani, C. B. Nasr, K. Sayin, M. Demiralp, U. Hasanova, G. Eyvazova, Z. Gakhramanova and V. Abbasov, *J. Iran. Chem. Soc.*, 2022, **20**, 1–15, DOI: [10.1007/s13738-022-02659-9](https://doi.org/10.1007/s13738-022-02659-9).

- 48 R. D. Dennington II, T. A. Keith and J. M. Millam, "Gauss-View 6.0.16", 2016, Wallingford, CT.
- 49 M. J. Frisch, G. W. Trucks, H. B. Schlegel, G. E. Scuseria, M. A. Robb, J. R. Cheeseman, G. Scalmani, V. Barone, G. A. Petersson, H. Nakatsuji, X. Li, M. Caricato, A. V. Marenich, J. Bloino, B. G. Janesko, R. Gomperts, B. Mennucci, H. P. Hratchian, J. V. Ortiz, A. F. Izmaylov, J. L. Sonnenberg, D. Williams-Young, F. Ding, F. Lipparini, F. Egidi, J. Goings, B. Peng, A. Petrone, T. Henderson, D. Ranasinghe, V. G. Zakrzewski, J. Gao, N. Rega, G. Zheng, W. Liang, M. Hada, M. Ehara, K. Toyota, R. Fukuda, J. Hasegawa, M. Ishida, T. Nakajima, Y. Honda, O. Kitao, H. Nakai, T. Vreven, K. Throssell, J. A. Montgomery Jr., J. E. Peralta, F. Ogliaro, M. J. Bearpark, J. J. Heyd, E. N. Brothers, K. N. Kudin, V. N. Staroverov, T. A. Keith, R. Kobayashi, J. Normand, K. Raghavachari, A. P. Rendell, J. C. Burant, S. S. Iyengar, J. Tomasi, M. Cossi, J. M. Millam, M. Klene, C. Adamo, R. Cammi, J. W. Ochterski, R. L. Martin, K. Morokuma, O. Farkas, J. B. Foresman and D. J. Fox, *Gaussian 16, Revision B.01*, Gaussian, Inc., Wallingford CT, 2009.
- 50 Schrödinger Release 2021-2: LigPrep, Schrödinger, LLC, New York, NY, 2021.
- 51 Schrödinger Release 2021-2: Maestro, Schrödinger, LLC, New York, NY, 2021.
- 52 Schrödinger Release 2021-2: QikProp, Schrödinger, LLC, New York, NY, 2021.
- 53 A. Samrot, S. Saigeetha, C. Mun, S. Abirami, K. Purohit, P. Cypriana, T. Stalin, L. Dhas, S. Inbathamizh and S. Kumar, *Sci. Rep.*, 2021, **11**, 24511, DOI: [10.1038/s41598-021-03328-2](https://doi.org/10.1038/s41598-021-03328-2).
- 54 S. Shah, Z. Chowdhury, M. Johan, R. Bin, I. Badruddin, H. Khaleed, S. Kamangar and H. Alrobei, *Molecules*, 2022, **27**, 789, DOI: [10.3390/molecules27030789](https://doi.org/10.3390/molecules27030789).
- 55 A. Azizi, *J. Inorg. Organomet. Polym. Mater.*, 2020, **30**, 3552–3561, DOI: [10.1007/s10904-020-01500-1](https://doi.org/10.1007/s10904-020-01500-1).
- 56 S. Al-Musawi, S. Albukhaty, H. Al-Karagoly, G. M. Sulaiman, M. S. Jabir and H. Naderi-Manesh, *Adv. Nat. Sci.: Nanosci. Nanotechnol.*, 2020, **11**(4), 045009, DOI: [10.1088/2043-6254/abc75b](https://doi.org/10.1088/2043-6254/abc75b).
- 57 S. Saqib, A. Nazeer, M. Ali, W. Zaman, M. Younas, A. Shahzad and M. Nisar, *Biometals*, 2022, **35**, 967–985, DOI: [10.1007/s10534-022-00417-1](https://doi.org/10.1007/s10534-022-00417-1).
- 58 J. Fishovitz, J. A. Hermoso, M. Chang and S. Mobashery, *IUBMB Life*, 2014, **66**(8), 572–577, DOI: [10.1002/iub.1289](https://doi.org/10.1002/iub.1289).
- 59 I. A. Myles and S. K. Datta, *Semin. Immunopathol.*, 2012, **34**, 181–184, DOI: [10.1007/s00281-011-0301-9](https://doi.org/10.1007/s00281-011-0301-9).
- 60 N. Lv, Q. Kong, H. Zhang and J. Li, *Bioorg. Med. Chem. Lett.*, 2021, **41**, 128001, DOI: [10.1016/j.bmcl.2021.128001](https://doi.org/10.1016/j.bmcl.2021.128001).
- 61 S. O. Jensen and B. R. Lyon, *Future Microbiol.*, 2009, **4**, 565–582, DOI: [10.2217/fmb.09.30](https://doi.org/10.2217/fmb.09.30).
- 62 M. W. Shalaby, E. M. E. Dokla, R. A. T. Serya and K. A. M. Abouzid, *Eur. J. Med. Chem.*, 2020, **199**, 112312, DOI: [10.1016/j.ejmech.2020.112312](https://doi.org/10.1016/j.ejmech.2020.112312).
- 63 D. J. Scheffers and M. G. Pinho, *Microbiol. Mol. Biol. Rev.*, 2005, **69**, 585–607, DOI: [10.1128/MMBR.69.4.585-607.2005](https://doi.org/10.1128/MMBR.69.4.585-607.2005).
- 64 E. Sauvage, F. Kerff, M. Terrak, J. A. Ayala and P. Charlier, *FEMS Microbiol. Rev.*, 2008, **32**, 234–258, DOI: [10.1111/j.1574-6976.2008.00105.x](https://doi.org/10.1111/j.1574-6976.2008.00105.x).
- 65 M. A. W. Shalaby, E. M. Dokla, R. A. Serya and K. A. Abouzid, *Eur. J. Med. Chem.*, 2020, **199**, 112312, DOI: [10.1016/j.ejmech.2020.112312](https://doi.org/10.1016/j.ejmech.2020.112312).